UNIVERSITÀ
DEGLI STUDI
DI UDINE

Università degli studi di Udine

Polarization switching and interface charges in BEOL compatible Ferroelectric Tunnel Junctions

Original

Availability:
This version is available http://hdl.handle.net/11390/1215985 since 2023-09-04T13:47:04Z

Publisher:

Published
DOI:10.1109/ESSDERC53440.2021.9631812

Terms of use:
The institutional repository of the University of Udine (http://air.uniud.it) is provided by ARIC services. The aim is to enable open access to all the world.

Publisher copyright

(Article begins on next page)

19 April 2024

Polarization switching and interface charges in BEOL compatible Ferroelectric Tunnel Junctions

R.Fontanini[(1)], J.Barbot[(2)], M.Segatto[(1)], S.Lancaster[(3)], Q.Duong[(3)], F.Driussi [(1)], L.Grenouillet[(2)], F.Triozon[(2)], J.Coignus[(2)], T.Mikolajick[(3,4)], S.Slesazeck[(3)], D. Esseni[(1)]

[(1)]DPIA, University of Udine, Udine, Italy; [(2)]CEA, LETI, Univ. Grenoble Alpes, Grenoble, France; [(3)] NaMLab gGmbH, Dresden, Germany; [(4)] Chair of Nanoelectronics, IHM, TU Dresden, Germany.

Abstract

We here report a joint experimental and theoretical analysis of polarization switching in ferroelectric tunnel junctions. Our results show that the injection and trapping of charge into the ferroelectric-dielectric stack has a large influence on the polarization switching. Our results are relevant to the physical understanding and to the design of the devices, and for both memory and memristor applications.

© 2021 IEEE. Personal use of this material is permitted. Permission from IEEE must be obtained for all other uses, in any current or future media, including reprinting/republishing this material for advertising or promotional purposes, creating new collective works, for resale or redistribution to servers or lists, or reuse of any copyrighted component of this work in other works.

I. Introduction

The rise of artificial intelligence has emphasized the need for hardware platforms specifically conceived for new computational paradigms, such as crossbar arrays for artificial deep neural networks [1], and hybrid memristive-CMOS circuits for spike-based neuromorphic computing [2]. Ferroelectric based CMOS electron devices offer promising options for memories, as well as for memristors capable of multiple resistance levels [3], [4].

Energy efficiency is a main target for neuromorphic computing and it is a major concern for all computational technologies [5], [6]. Thanks to the field driven polarization switching, Ferroelectric Tunnel Junctions (FTJs) can provide high impedance and low energy synaptic devices, and a four level operation has been demonstrated in a Metal-Ferroelectric-Dielectric-Metal (MFIM) structure [7]. In ferroelectric-dielectric (FE-DE) systems, charge injection through the thin dielectric and charge trapping are expected to play a prominent role for the switching and stabilization of the polarization [8]. In fact, large interface charge

densities have been reported in both for FeFETs [9] and MFIM structures [10], albeit some quantitative aspects are still debated [11].

In this paper we present a joint effort based on experiments and comprehensive numerical modelling to investigate the role of polarization switching, charge trapping and depolarization effects in TiN/$HfZrO_4$/Al_2O_3/TiN CMOS compatible FTJs. Our results help in clarifying the physical operation of the devices and provide a sound basis for the device design.

II. Device fabrication

Large area (7850 μm^2) FTJ structures were fabricated, featuring TiN top- and bottom-electrodes, an aluminium oxide (Al_2O_3) tunnelling layer at the top electrode interface and a 10 nm thick hafnium zirconium oxide ($HfZrO_4$) ferroelectric between the bottom electrode and the tunnelling layer. The Al_2O_3 layer thickness was varied between 1.5 nm and 2.0 nm. The TiN electrodes were deposited by physical vapor deposition at 350°C. Figure 1(a) reports a high resolution TEM cross section of the device. Prior to the HZO deposition, the TiN bottom electrode underwent chemical mechanical polishing (CMP) to improve roughness (rms= 0.1 nm). Both oxide layers were deposited by atomic layer deposition at 280°C. The maximum thermal budget for all structures was 450°C.

III. Models and comparison to experiments

The ferroelectric dynamics and electrostatics of an FTJ with the structure illustrated in Fig. 1(b) were self-consistently solved by using the multi-domain Landau, Ginzburg, Devonshire (LGD) model thoroughly described in [12], [13]. The nominal values for the anisotropic constants used in simulations are α=$-1.1\cdot 10^8$[m/F], β=$-1.5\cdot 10^{10}$[m^5/F/C^2], γ=$1.85\cdot 10^{11}$[m^9/F/C^4] , which result in a remnant polarization $P_r \approx 24$ μC/cm^2 and coercive field $E_c \approx 1.8$ MV/cm, that are in fairly good agreement with polarization-voltage response of MFM samples [14]. Our simulations typically include n_D=100 domains, and we account for domain to domain random variations of α, β, γ (see Tab.I).

In our model the depolarization energy and fields are described by duly accounting for the three-dimensional nature of the electrostatics in the device. At each time t and external bias $V_B(t)$, the LGD equations provide the domain polarization $P_i(t)$, the electric fields in the ferroelectric $E_{F,i}$ and in the dielectric $E_{D,i}$, and thus the band diagram in each domain (with i=$1, 2\cdots n_D$) [13].

Figure 2 compares simulations and experiments for the P-V curve obtained during the P and N pulses of a "Positive-Up-Negative-Down" (PUND) measurement and for a t_D=1.5 nm thick Al_2O_3 layer. The

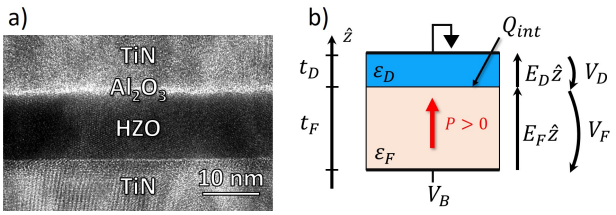

Figure 1: a) High resolution TEM cross section of the TiN/1.5 nm Al_2O_3/10 nm HZO/TiN devices used in experiments; b) Sketch of the device template for numerical simulations.

Table I: Material parameters employed in simulations: ε_r is the relative permittivity, and χ, Φ_M are respectively the electron affinities of the dielectrics and the TiN workfunction. Calculations include domain to domain variations of α_i, β_i, γ_i parameters (with i=1, 2 $\cdots$ n_D), corresponding to a ratio σ_{EC} = 10% between the standard deviation and the mean value of the coercive field E_C. The resistivity for the ferroelectric is ρ=112Ωm which is consistent with recently reported values for HZO based capacitors [15].

Material	Thick.[nm]	χ[eV]	ε_r [$ad.$]	Φ_M [eV]
$HfZrO_4$	10	2.4	34	-
Al_2O_3	1.5, 2	1.4	10	-
TiN	-	-	-	4.55

Table II: Material parameters related to tunnelling and trapping in TiN/$HfZrO_4$/Al_2O_3/TiN FTJs. The energy cross-section σ_E was set to $7meV$ in all simulations. Acceptor and donor type traps are uniformly distributed in energy respectively from 0.6 to 2.6eV and from 1.8 to 3.8eV below the HZO conduction band, respectively (see also Fig. 4).

t_D	$\sigma_{T,acc}$ [cm^2]	$\sigma_{T,don}$	m_D [m_0]	m_F
1.5 nm	$2.5 \cdot 10^{-16}$	10^{-16}	0.2	0.4
2.0 nm	$5 \cdot 10^{-15}$	10^{-15}	0.15	0.4

PUND method consists of a series of triangular pulses (see also inset in Fig. 3) and it is widely used in the characterization of ferroelectric devices [16]. In this work we used a 10kHz PUND with a delay time of 5ns between each pulse. The wake-up of the experimental results was done by bipolar triangular cycling (1000 cycles - 100kHz frequency) with a maximal voltage the same as the PUND.

As shown in Fig. 2 and 3, simulations neglecting any trapped charge at the FE-DE interface (or inside the dielectrics) result in much more stretched P-V curves compared to experiments. These simulations are instead consistent with the experimental P-V curves reported for an HZO capacitor serially connected to a discrete ceramic capacitor, that ensures a negligible charge injection through the dielectric [8].

Figure 3 illustrates the I-V curves during the P and N pulses corresponding to the same measurements as in Fig. 2. In simulations with no traps the displacement current $C_S(\partial V_B/\partial t)$, due to the linear polarization

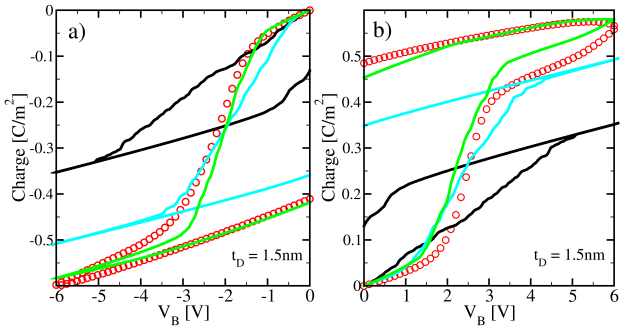

Figure 2: Polarization versus voltage characteristics measured by the PUND method for a 50 μs width of the triangular pulse (see inset in Fig. 3) and for an Al_2O_3 FTJ with t_D=1.5 nm. Results are reported for the P pulse (a), and for the N pulse (b). Corresponding simulations are shown for no trapped charge (black solid line), and for different equivalent areal density of acceptor and donor type traps.

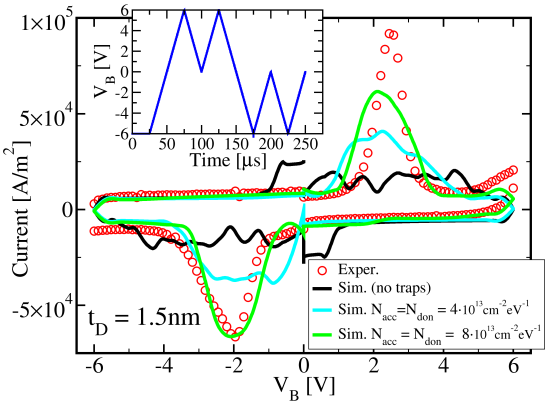

Figure 3: Current versus voltage characteristics corresponding to the PUND measurements in Fig. 2.

response, is reproduced well (with C_S=$[1/C_D+1/C_F]^{-1}$ and C_D=$\varepsilon_0\varepsilon_D/t_D$, C_F=$\varepsilon_0\varepsilon_F/t_F$), but the simulated switching current ($\partial P/\partial t$) is spread over a large voltage range and no peak clearly exceeding the $C_S(\partial V_B/\partial t)$ contribution can be observed in simulations. This feature is again in stark disagreement with experiments.

The discrepancies between simulations and experiments in Figs. 2 and 3 suggest that charge injection and trapping in the dielectric stack plays an important role in the polarization switching for the FTJs, when considering the small dielectric thickness [8]. Hereafter we will assume that conduction in the Al_2O_3 layer is limited by tunnelling, even if transport mechanisms assisted by defects through Poole-Frenkel and hopping mechanisms are also possible in thin oxides [17]. We assume that the most important trapping effects for the polarization switching occur close to the FE-DE interface, and thus we describe the trap density and trapped charge in terms of areal densities. However, it is understood that these figures should be regarded as equivalent areal densities possibly summarizing also a charge trapping in the DE and FE films.

Acceptor and donor type traps at the FE-DE interface were described according to a first order dynamic equation. In particular, if we denote by f_T the occupation of the trap at energy E_T and with c_{MD0}, c_{MF0} the capture rate from the metal MD and MF electrodes contacting respectively DE and FE (see Fig. 4), then f_T is governed by the following equation:

$$\frac{\partial f_T}{\partial t} = c_{MD0}\,[\,f_{0,MD} - f_T\,] + c_{MF0}\,[\,f_{0,MF} - f_T\,]\,, \tag{1}$$

where $f_{0,M}(E_T)$=$1/[1+\exp((E_T-E_{f,M})/(K_BT))]$ is the Fermi occupation function in the metal electrodes, with $E_{f,MF}$=$E_{f,MD}-qV_B$. In the derivation of Eq. 1 we used a detailed balance condition, ensuring that the steady state f_T value at the equilibrium (i.e. for V_B=0V) is given by the Fermi function. The capture rates can be expressed in terms of the tunnelling transmission between the FE-DE interface and each terminal MD or MF according to:

$$c_{M-0}(E_T) = \sigma_T\sigma_E\frac{m_{\|}}{2\pi^2\hbar^3}\int_0^{+\infty} T_{M-}(E_T-\varepsilon)d\varepsilon, \tag{2}$$

where $\sigma_T[1/\mathrm{m}^2]$, $\sigma_E[1/\mathrm{eV}]$ are respectively an area and an energy cross section of the traps.

Equation 2 assumes an effective mass approximation in the metal electrodes[1] and an energy separability

[1]Here $m_{\|}$ corresponds to an effective mass for the density of states of the metals. In the lack of a better $m_{\|}$ determination, in calculations we used the popular assumption $m_{\|} \approx m_0$ [20].

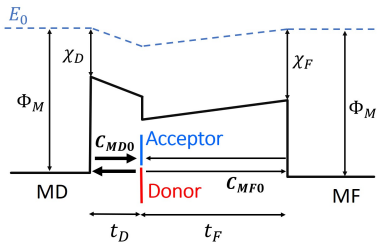

Figure 4: Sketch of the band diagram in the TiN/$HfZrO_4$/Al_2O_3/TiN stack, showing also the energy position of acceptor and donor type traps. The capture rates c_{MD0}, c_{MF0} are also pictorially illustrated as electron fluxes from the electrodes to the traps.

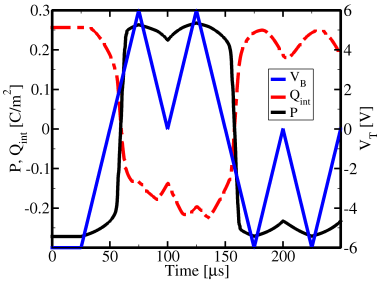

Figure 5: Polarization, P, and interface charge, Q_{int}=Q_{acc}+Q_{don}, versus time during for the same PUND simulations as in Figs.2, 3. The Al_2O_3 thickness is t_D=1.5 nm and the trap densities are $N_{acc} = N_{don} = 8 \cdot 10^{13}$ [1/(cm^{2}eV)]. The V_B waveform is also shown (blue line).

E=$E_\perp$+$\varepsilon(\mathbf{k})$, with the transverse energy $\varepsilon(\mathbf{k})$ being conserved in the tunnelling process [18]. The tunnelling transmission $T_{MD}(E_T - \varepsilon)$ and $T_{MF}(E_T - \varepsilon)$ were calculated through the WKB approximation, with the effective tunnelling masses m_D, m_F, and energy barriers Φ_D=$(\Phi_{TiN} - \chi_D)$, Φ_F=$(\Phi_{TiN} - \chi_F)$ in Tabs. I and II. More details about the tunnelling model may be found in [19]. The charges Q_{acc}, Q_{don} trapped in acceptor and donor traps, respectively, can be written as:

$$Q_{acc} = \frac{(-q)}{n_D} \sum_{E_T} N_{acc}\, f_T(E_T)\, \Delta E, \tag{3a}$$

$$Q_{don} = \frac{q}{n_D} \sum_{E_T} N_{don}\, \left(1 - f_T(E_T)\right)\, \Delta E, \tag{3b}$$

where N_{acc}, N_{don} denote the trap densities and ΔE is the energy step between the discrete trap levels. Equations 1 to 3 refer to a single domain in the FTJ structure, and Eq. 1 was solved in all domains and self-consistently with the LGD equations for the ferroelectric dynamics.

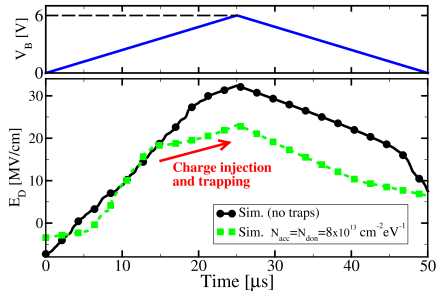

Figure 6: Electric field across the Al_2O_3 layer during the P pulse analyzed in Fig. 2(a), hence for t_D=1.5 nm.

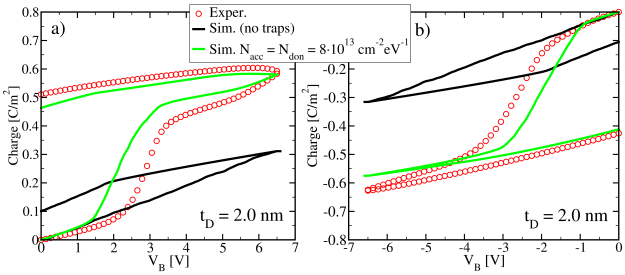

Figure 7: Measured and simulated P-V curves for a PUND waveform as in Fig. 2, but for an Al_2O_3 FTJ with t_D=2.0 nm.

Figure 2 suggests that simulations can be reconciled with experiments only by assuming a large equivalent trap density, and Fig. 3 shows that the corresponding simulated I-V plot can also track quite well the coercive voltage and the shape of the measured current. Figure 5 offers a simulation based insight about the behaviour of the average polarization and interface charge (P and Q_{int}, both averaged over the device area) along a PUND waveform. In this example both positive and negative P are compensated by Q_{int} to a large extent. This is the basic mechanism by which the depolarization field can be reduced compared to the case with $Q_{int} \approx 0$, and the simulated P-V curves reconciled with experiments. Figure 6 also reports the simulated field, E_D, across the Al_2O_3 layer during the P pulse analyzed in Fig. 2(a). In simulations with no traps, E_D exceeds 30 MV/cm at the V_B peak, which is an unrealistically large value and would also lead to a huge tunnelling current. In the presence of traps, instead, when E_D exceeds approximately 15 MV/cm electrons are injected through the dielectric and trapped at the FE-DE interface. The resulting building up of negative charge quenches the increase of E_D, as pointed out in [8].

Figure 7 shows that the results are qualitatively similar for the FTJs having a slightly thicker Al_2O_3 layer. Even for $t_D = 2.0$ nm the simulations with no traps are in sharp disagreement with experiments. Moreover, the same trap densities result in a fairly good agreement with P-V and I-V curves for both $t_D = 1.5$ nm and 2.0 nm.

The experiments in Fig. 2 and 7 suggest that, if it is the charge injection through Al_2O_3 that feeds the charge trapping at the FE-DE interface, then such an injection must be similarly effective for $t_D = 1.5$ nm and 2.0 nm. To obtain this behaviour in our tunnelling based model, for the t_D=2.0 nm case it was necessary to increase the trap cross section σ_T and slightly decrease the Al_2O_3 tunnelling mass (see Tab.I). The need for an empirical adjustment of these parameters may suggest that additional transport mechanisms are involved in Al_2O_3 [17].

IV. Implications for the design of FTJs

The results of the previous section suggest that charge injection and trapping play an important role in the polarization switching and stabilization in the MFIM based FTJs at study. As a corollary, we found that the interface charge has implications for different aspects of the device design. Figure 8, for example, examines the polarization loss at $V_B = 0$ V after the N pulse of a PUND sequence, which is linked to detrapping. In the simulations of Fig. 8, in fact, a fraction of the donor traps that have positively charged during the N pulse lie below the Fermi level when V_B goes back to zero. During the retention at $V_B = 0$ V such donor

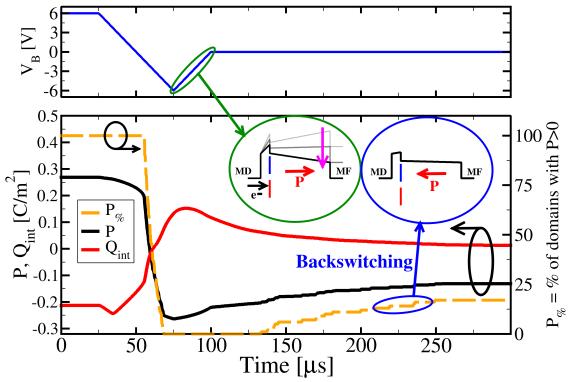

Figure 8: Polarization (black line) and interface charge (red line) during an N pulse and the following retention phase at $V_B = 0$ V. The percentage of positive polarization domains (yellow dashed line, right y axis) increases during the retention phase. Insets show the band diagram for negative (left) and a backswitched (right) polarization configurations.

traps capture electrons and thus become neutral (see Eq.1). The resulting reduction of the positive interface charge $Q_{int} \approx Q_{don}$ enhances the depolarization field, which eventually leads to the back-switching of a fraction of domains. Of course the behaviour in Fig. 8 is critically influenced by the position of the trap energy levels. However, a similar interplay between detrapping and back-switching is plausible in actual devices.

V. Conclusions

We have shown through a comparison between experiments and simulations that the polarization switching in MFIM based FTJs is greatly influenced by the injection and trapping of charge into the dielectric stack, which compensates the ferroelectric polarization to a large extent. In this paper we have described this behaviour in terms of tunnelling injection through the thin Al_2O_3 layer and trapping at the FE-DE interface. However, defects assisted transport through the dielectrics and charge trapping in the HZO film may also contribute to the picture. The understanding and control of such a charge compensation is crucial for the design of this class of FTJs.

Acknowledgements: This work was supported by the European Union through the BeFerroSynaptic project (GA:871737).

References

[1] Shimeng Yu, "Neuro-inspired computing with emerging nonvolatile memories", *Proc. of IEEE*, vol. 106, n. 2, p. 260, 2018.

[2] E. Chicca, G. Indiveri, "A recipe for creating ideal hybrid memristive-CMOS neuromorphic processing systems", *Appl. Phys. Lett.*, vol. 116, p. 120501, 2020.

[3] T. Mikolajick *et al.*, "Next Generation Ferroelectric Memories enabled by Hafnium Oxide" *IEDM Tech. Dig.*, p.15.5.1, 2019.

[4] S. Slesazeck, T. Mikolajick, "Nanoscale resistive switching memory devices: a review", *Nanotech.*, vol. 30, p. 352003, 2019.

[5] A.M.Ionescu, H.Riel,"Tunnel field-effect transistors as energy-efficient electronic switches", *Nature*, p. 329, 2011.

[6] D. Esseni, M. Pala, P. Palestri, C. Alper, T. Rollo, "A review of selected topics in physics based modeling for tunnel field-effect transistors" *Semic. Science and Techn.*, vol. 32, p. 083005, 2017.

[7] B. Max, M. Hoffmann, S. Slesazeck and T. Mikolajick, "Direct Correlation of Ferroelectric Properties and Memory Characteristics in Ferroelectric Tunnel Junctions" *Journal of Electr. Dev. Soc.*, vol. 7, p. 1175, 2019.

[8] H. W. Park *et al.*, "Polarizing and depolarizing charge injection through a thin dielectric layer in ferroelectric-dielectric bilayer", *Nanoscale*, vol. 13, pp. 2556-2572, 2021.

[9] K. Toprasertpong, M. Takenaka, S. Takagi, "Direct Observation of Interface Charge Behaviors in FeFET by Quasi-Static Split C-V and Hall Techniques: Revealing FeFET Operation", *IEDM* 2019 pp. 23.7.1-23.7.4.

[10] J. Li, Y. Qu, M. Si, X. Lyu, P.D. Ye, "Multi-Probe Characterization of Ferroelectric/Dielectric Interface by C-V, P-V and Conductance Methods" *Symp. VLSI tech.*, 2020.

[11] S. Deng *et al.*, "Examination of the Interplay Between Polarization Switching and Charge Trapping in Ferroelectric FET", *IEDM* 2020, pp. 4.4.1-4.4.4.

[12] T. Rollo, F. Blanchini, G. Giordano, R. Specogna, D. Esseni, "Revised analysis of negative capacitance in ferroelectric-insulator capacitors: analytical and numerical results, physical insight, comparison to experiments.", *IEDM* 2019, p. 7.2.1.

[13] T. Rollo, F. Blanchini, G. Giordano, R. Specogna, D. Esseni "Stabilization of negative capacitance in ferroelectric capacitors with and without a metal interlayer", *Nanoscale*, vol. 12, pp. 6121–6129, 2020.

[14] R. Alcala *et al.*, "Influence of oxygen source on the ferroelectric properties of ALD grown $Hf_{1-x}Zr_xO_2$ films", *J. Phys. D: Appl. Phys.*, vol. 54, p. 035102, 2021.

[15] T. Kim, J. A. del Alamo, D.A. Antoniadis, "Dynamics of HfZrO2 Ferroelectric Structures: Experiments and Models", *IEDM* 2020, pp. 21.4.1-21.4.4.

[16] K.M. Rabe, M. Dawber, C. Lichtensteiger, C.H. Ahn, J.M. Triscone, "Physics of Ferroelectrics", Topics in Applied Physics, vol 105, p. 2, 2007.

[17] H. Scrhöder, "Poole-Frenkel-effect as dominating current mechanism in thin oxide films—An illusion?", *Journal Applied Physics* 117, p. 215103, 2015.

[18] S. Takagi, N. Yasuda, A. Toriumi, "Experimental evidence of inelastic tunneling in stress-induced leakage current", *IEEE Trans. on Elec. Dev.*, vol. 46, pp. 335-341, 1999.

[19] R. Fontanini, M. Massarotto, R. Specogna, F. Driussi, M. Loghi, D. Esseni, "Modelling and Design of FTJs as High Reading-Impedance Synaptic Devices", *EDTM* 2021 (in press).

[20] F. Driussi, P. Palestri, L. Selmi, "Modeling, simulation and design of the vertical Graphene Base Transistor", *Micro. Eng.* 109, pp. 338-341, 2013.